

## CFD-BASED ANALYSIS OF THE 14-BIS AIRCRAFT AERODYNAMICS AND STABILITY

**Leonardo Ostan Bitencourt**

Instituto Tecnológico de Aeronáutica, CTA/ITA/IEA, São José dos Campos  
lostan@gmail.com

**Ramon Morais de Freitas**

Instituto Nacional de Pesquisas Espaciais, INPE, São José dos Campos  
ramon@dsr.inpe.br

**Grégori Pogorzelski**

Instituto Tecnológico de Aeronáutica, CTA/ITA/IEA, São José dos Campos  
gpogor@gmail.com

**João Luiz F. Azevedo**

Instituto de Aeronáutica e Espaço, CTA/IAE/ASA-L, São José dos Campos  
azevedo@iae.cta.br

***Abstract.** The year 2006 marks the centennial of the historical, heavier-than-air flight by Alberto Santos Dumont with his 14-Bis aircraft. On October 1906, at the Bagatelle Field, in Paris, France, Santos Dumont flew the 14-Bis aircraft and won the Deutsch-Archdeacon Prize. The aircraft had a complex canard-biplane configuration, based on Hargrave's box kites. In this context, the present work describes the results of a CFD-based analysis of the 14-Bis aircraft aerodynamics and flight stability. The 14-Bis aircraft CAD geometry was generated from historical resource observations. CFD computations are performed using well-established commercial and proprietary codes for calculation of the historical flight conditions. The computations consider a Reynolds-averaged Navier-Stokes formulation, in which turbulence closure is achieved using Menter's SST model. The calculations consider unstructured grids and the codes feature a multigrid method for convergence acceleration. The flight conditions investigated are primarily concerned with historical observations regarding flight speeds and the need for a more powerful engine, as well as flight stability characteristics of the 14-Bis airplane, which are unknown up to the present day. The results lead to qualitative agreement with historical reports, although quite interesting conclusions can be drawn with regard to actual aerodynamic flight speeds and aircraft stability parameters.*

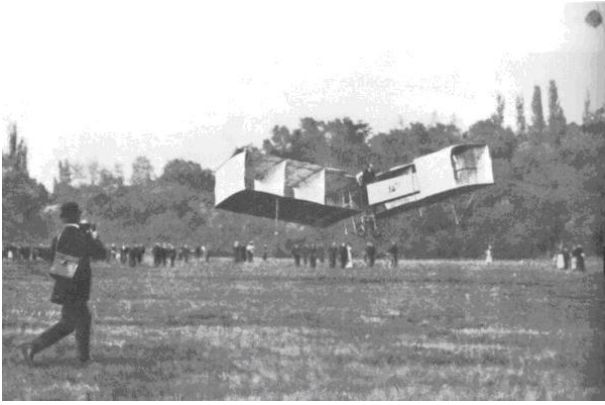
***keywords:** Aerodynamics, CFD, Centennial of Flight, Santos Dumont, 14-Bis*

### 1. Introduction

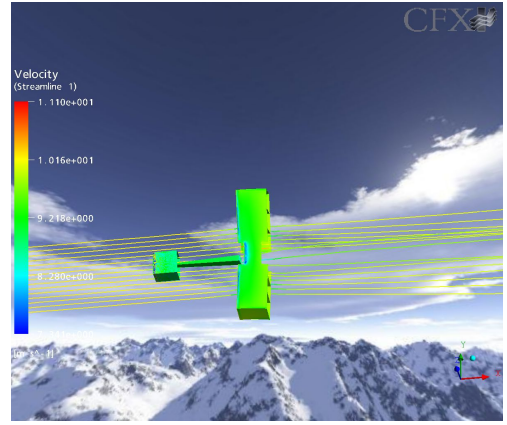
Alberto Santos-Dumont, native from Brazil, was a genius obsessed with the idea of flight. First working on balloons and dirigibles, and latter designing engine-powered vehicles, he became one of the best-known men in Paris. On October 23, 1906, in the Bagatelle Field, Paris, France, Santos Dumont flew the 14-Bis aircraft and won the Deutsch-Archdeacon Prize. The 14-Bis aircraft was constructed from pine and bamboo poles covered with Japanese silk. The aircraft had a complex canard-biplane configuration, which was a construction based on Hargrave's box kites. The Hargrave cell in the nose pivoted up and down to act as an elevator and from side to side in the role of a rudder. The wings were rigged with 10 deg. of dihedral and the first flights were made without ailerons. The preliminary flight test happened with the 14-Bis aircraft attached to the No 14 dirigible, which explains its designation.

The 14-Bis flew without the dirigible on September 13, 1906, making a hop between 6 and 13 meters. According to an article published in Pegasse magazine, after having achieved partial success in his flight attempt, Santos Dumont identified possible problems with the 14-Bis configuration, and performed the following improvements:

- Elevation of the gas tank;
- Application of varnish on the silk to diminish the porosity;



(a) 14-Bis in flight 23 October 1906 - Source: Museu Aeroespacial.



(b) CFD simulated model over the mountains.

Figure 1: The historical first flight and a CFD simulated model.

- Taking the back wheel off;
- Decrease of the wing incidence angle;
- Upgrade of the original power-plant, replacing the Antoinette 24 hp engine by a 50 hp version.

On October 23, Santos Dumont managed to fly for 60 meters as illustrated in the left of Fig. 1. Then, on November 12, he flew 220 meters in 21 1/2 seconds with members of the Aero-Club de France in attendance. Santos Dumont won a prize of 1500 francs for making the first flight over 100 meters in Europe. Since he was observed by officials from what would become the Federation Aeronautique Internationale, Santos Dumont was credited with making the first heavier-than-air powered flight. The main 14-Bis geometric characteristics are presented in Tab. 1.

Table 1: Historical 14-Bis geometric characteristics.

|  |                   |                                |                      |
|--|-------------------|--------------------------------|----------------------|
| Total Canard Area                                      | 8 m <sup>2</sup>  | Length                         | 10 m                 |
| Canard Chord   | 2 m               | Engine Power                   | 24 hp(first) - 50 hp |
| Canard Span  | 2 m               | Weight with Pilot              | ≈ 315 kg             |
| Wing Chord   | 2.5 m             | Historical Cruise Flight Speed | 9 to 12 m/s          |
| Wing Span  | 11.50 m           | Wing Chord Reynolds Number     | 10 <sup>6</sup>      |
| Wing Dihedral  | 10 deg.           | Canard Chord Reynolds Number   | 10 <sup>7</sup>      |
| Total Wing Area  | 50 m <sup>2</sup> | Canard-Wing Distance           | 5 m                  |
| Center of Gravity ( $X_{cg}$ ) Estimate <sup>(1)</sup> | 7.5 m             |                                |                      |

<sup>(1)</sup>: Reference point is aircraft nose.

During a long time, there were only two approaches for aerodynamic studies, wind tunnel testing and analytical solution of simplifications to the Navier-Stokes equations. The last method is very limited, since only some simple cases can be predicted with acceptable accuracy. The wind tunnel also has some disadvantages, such as high energy consumption, and a considerably large time spent constructing the model, performing the tests, and processing the data. Moreover, only some flow conditions can be reproduced. It must be pointed that those factors together are related to more costs.

Computational fluids dynamics (CFD) techniques emerge as an alternative able to reduce project costs, since time and money spent with wind tunnel testing are substantially reduced. In addition to this, CFD has the advantage of numerically solving the fluid equations in the entire flowfield, thus allowing for local analysis of the flow properties in a way much more detailed than any wind tunnel visualization techniques could show. But, in spite of CFD advantages, wind tunnel tests still are an indispensable stage of every aircraft project, since this is as similar to physical reality as possible.

The main objective of this article is to apply CFD techniques for aerodynamic analyses of the 14-Bis aircraft. The central idea is to compute lift and drag curves for this aircraft, at the presumed flight conditions, and then assess and clarify some controversial points regarding stability, flight speed, ground effect and power plant performance. The study will also explore angle of attack and velocity variations around the historical flight conditions.

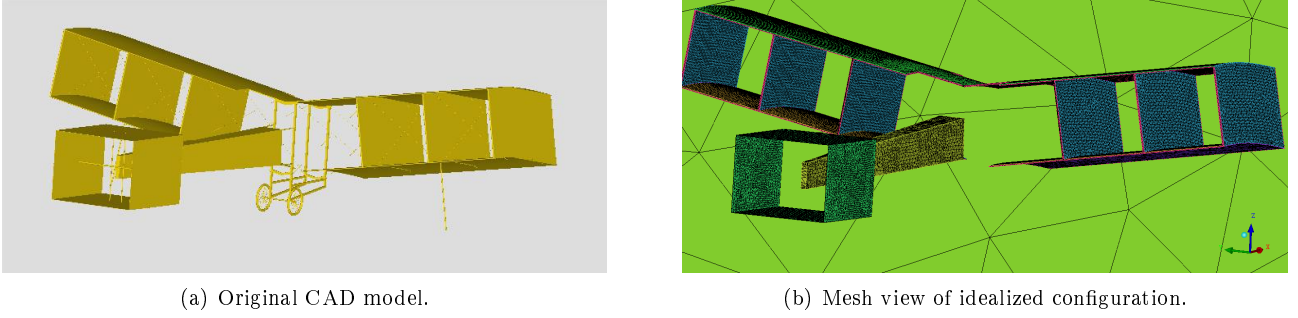


Figure 2: Comparative view of the original CAD model and simulated configuration.

## 2. Theoretical Formulation

### 2.1. Reynolds-Averaged Navier-Stokes Equations

These equations constitute the more general flow formulation for which the fluid continuum hypothesis can be assumed. The Navier-Stokes equations, for a perfect gas, without the generation of heat and with negligible field forces can be written as

$$\frac{\partial \rho}{\partial t} + \frac{\partial(\rho u_j)}{\partial x_j} = 0 \quad , \quad (1)$$

$$\frac{\partial(\rho u_i)}{\partial t} + \frac{\partial(\rho u_i u_j)}{\partial x_j} + \frac{\partial p}{\partial x_i} - \frac{\partial \tau_{ij}}{\partial x_j} = 0 \quad , \quad (2)$$

$$\frac{\partial e}{\partial t} + \frac{\partial[(e + p) u_j - \tau_{ij} u_i + q_j]}{\partial x_j} = 0 \quad , \quad (3)$$

where  $\rho$ ,  $p$  and  $\vec{u}$  are the fluid density, pressure and velocity, respectively,  $\vec{\tau}$  is the viscous stress tensor,  $\vec{q}$  is the heat flux vector and  $t$  is the time. The term  $e$  is the total energy per unit of volume, given by

$$e = \rho \left[ e_i + \frac{1}{2}(u^2 + v^2 + w^2) \right] \quad , \quad (4)$$

where  $u$ ,  $v$  and  $w$  are the velocity vector Cartesian components and  $e_i$  is the internal energy.

In the formulation, two assumptions were adopted: the absence of heat transfer, i.e., the heat flux vector terms equal zero, and the flow was treated as incompressible due to the low flow Mach number values (lower than 0.05). To save computational memory and processing capabilities, the turbulent flow analyses are performed using the Reynolds-averaged Navier-Stokes equations. These equations contain the mean variables and a certain number of terms representing the turbulence effects that must be modeled.

## 3. Numerical Approach

### 3.1. Flow Solver

The computations on unstructured grids have been carried out by CFX (2005) which is a software capable of performing the analysis and solution of complex internal and external three dimensional flows. The solutions of the turbulent flow regions were based on the Reynolds-averaged Navier Stokes equations (RANS), supported by Menter's SST turbulence model (Menter, 1994).

The CFX solver simulated a steady, viscous and incompressible flow around the 14-Bis model. This code uses a cell-vertex, finite element-based control volume method. An iterative, second order, time marching scheme is used to numerically solve the RANS equations. To decrease the computational time, some convergence acceleration techniques, such an algebraic multigrid (MG) procedure, and parallel computations are used during the simulations.

### 3.2. Grid Generation

The 14-Bis CAD geometry was generated from planform and historical source observations and it was provided by Prof. Greco’s research group at University of São Paulo, São Carlos campus. Around the geometry, the flow domain was discretised using unstructured grids. Since memory and processing capabilities were limited, the geometry was simplified keeping only the main components, i.e., wings, canard and fuselage. Figure 2 makes a parallel between the original geometry and the simulated one.

The grid generator software used (ICEM-CFD, 2005) allows the automatic generation of the tetrahedral grid. However the superficial mesh over the airplane had a poor arrangement. The strategy adopted was to first create a structured 2-D grid over the geometric surface, and, after that, the Delauney method (Field, 1987) was applied, generating the desired unstructured volumetric grid. The element transitions were performed gradually to assure faster convergence and good solutions. Furthermore, regions of leading edges, trailing edges and the ones probably containing wakes received grid refinement to avoid spurious solutions.

### 3.3. Boundary Conditions

The correct application of boundary conditions is vital to properly close the numerical problem, assuring correct modeling. For the 14-Bis aircraft simulation, basically four different boundary conditions are used: INLET, OUTLET, OPENING, SLIP WALL and NO-SLIP WALL. The nomenclature used here is the same adopted by the CFX solver.

INLET condition is applied on the computational domain entrance surface where the freestream velocity magnitude and its direction are specified. NO-SLIP WALL condition assures that neither tangential nor normal velocity are present on the aircraft surface. The OUTLET condition is used to model the fluid flow exit in the domain. The OPENING condition models a boundary condition which permit entrance and exit of fluid freely. SLIP WALL condition is used on the surface just below the airplane in the simulations concerned about the the ground effect verification. For all the other test cases, the boundary treatment of that surface considered the OPENING condition. All boundary conditions prescribed are listed in Table 2.

Table 2: Detailed description of prescribed boundary condition on domain surfaces.

| Surface       | Type         | Description   |
|---------------|--------------|---|
| Aircraft      | NO-SLIP WALL | The normal and tangential velocity components are kept zero.              |
| Ground        | SLIP WALL    | On the surface below the airplane, the normal velocity component is zero. |
| Entrance      | INLET        | Entrance conditions are specified to the freestream conditions.           |
| Exit          | OUTLET       | The atmospheric pressure is specified as exit pressure.                   |
| Lateral sides | OPENING      | The atmospheric pressure is specified.                                    |

### 3.4. Post-Processor for Aerodynamics Forces

The post-processor, by means of simple and useful tools, allows evaluation of aerodynamics forces and the observation of the flow field variables, for example, pressure contours, streamlines or boundary layer velocity profiles. The resultant force in the airplane, when projected into the wind axis results in drag, lift and yaw forces. The evaluation of these aerodynamic forces is performed by integrating the surface pressure forces and shear stresses as shown in Eq. 5. More detailed description of these method can be found in Cummings *et al.* (1996).

$$\vec{F}_{near} = \int_{S_{near}} \left[ (p - p_{\infty}) \vec{I} - \vec{\tau} \right] \cdot \vec{n} dS \quad . \quad (5)$$

The aerodynamic drag is a force exerted by the flowfield on the body surface in a direction contrary to its movement in the air. The drag is the summation of the tangential, or skin friction forces, and surface pressures or normal forces, projected into the freestream direction.

By evaluating forces and moments over the airplane for several flight conditions, *i.e.*, varying the angle-of-attack ( $\alpha$ ), or the canard angle ( $\delta p$ ), the authors were able to extract important aerodynamics coefficients, and draw conclusions about the 14-Bis flight condition and possible stability range.

#### 4. Test Cases

The chosen test cases try to explore the main aerodynamic characteristics of the 14-Bis airplane. This is done through a parametric study shown in Table 3. The freestream velocity variation permits attest the invariability of the aerodynamic coefficients with the flight speed.

The simulations, including angle of attack (AoA) and canard deflection excursions, allow for estimates in lift, drag and pitching moment derivatives. Assuming steady level flight and using the estimated aerodynamic derivatives and coefficients, a possible flight condition could be estimated. Moreover, the ground effect influence is checked out varying the distance of the airplane from the ground.

Table 3: Simulated test cases for the parametric study of the main aerodynamic characteristics of the 14-Bis airplane.

| Set | Parameter  | Description       | Variation      | General Conditions  |
|-----|------------|-------------------|----------------|---|
| 1   | $V_\infty$ | Velocity          | 7.5 to 14 m/s  | Variation of $V_\infty$ , $\alpha = 0$ deg., $\delta_p=0$ .   |
| 2   | $\alpha$   | Angle of Attack   | -5 to +6 deg.  | Variation of $\alpha$ , $V_\infty = 11.5m/s$ , $\delta_p=0$ . |
| 3   | $\delta_p$ | Canard Deflection | 0 to +7.5 deg. | Variation of $\delta_p$ , $\alpha$ kept zero.                 |
| 4   | $\beta$    | Sideslip angle    | +1 to +7 deg.  | Variation of $\beta$ , $\alpha = 5$ deg.                      |
| 5   | $\Delta$   | Ground Distance   | 0 to 6 m       | Variation of $\Delta$ , $\alpha = 5$ deg.                     |

It is worth noting that all the test cases with fixed speed had the value 11.5 m/s adopted as default. That is because 11.5 m/s is an intermediate speed between the historical report of 10.21 m/s and the previously estimated value using numerical simulations (Bitencourt *et al.*, 2005). It is also important to mention that all the moment coefficients were calculated in relation to an estimated center of gravity (CG) position (Greco and Ribeiro, 2003). Its horizontal position was estimated at a point lying around 7.5 m from the airplane canard frontal extremity. The CG vertical position was estimated to be on the fuselage centerline.

#### 5. Results and Discussion

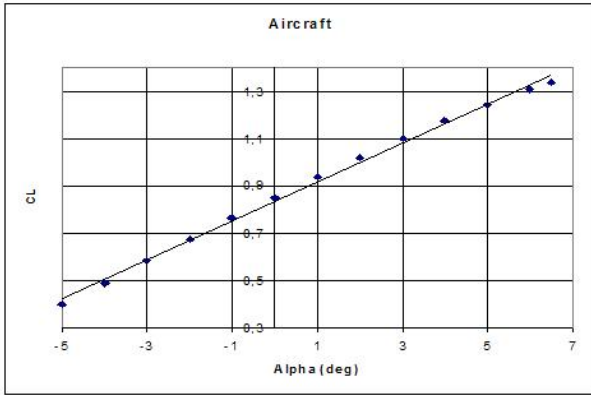
Results obtained for the first set of test cases (see Table 3) verified an expected absence of flight speed influence over the aerodynamic coefficients. The results show a maximal relative difference of 0.29% for  $C_L$ , 2.48% for  $C_D$  and 1.09% for  $C_m$ , in the speed range analyzed. Those small variations indicated that the aerodynamic coefficients can be considered independent of the flight speed. This hypothesis supports the use of a linear aerodynamic model, when performing flight dynamics and performance estimates in a range of flight speeds around the historical value.

The second and third sets of test cases (see Table 3) led to obtaining the aerodynamic coefficients and derivatives needed to perform an analysis of the aircraft longitudinal behavior. Figure 3 shows the  $C_L \times \alpha$ ,  $C_m \times \alpha$ ,  $C_D \times C_L$  and  $L/D \times \alpha$  curves that were obtained for the whole aircraft. The authors would like to note that all coefficients presented here were made dimensionless using the wing planform area and the wing mean chord. Figure 4 shows the  $C_m \times \delta_p$  and  $C_L \times C_{\delta_p}$  curves which are necessary for extraction of control derivatives.

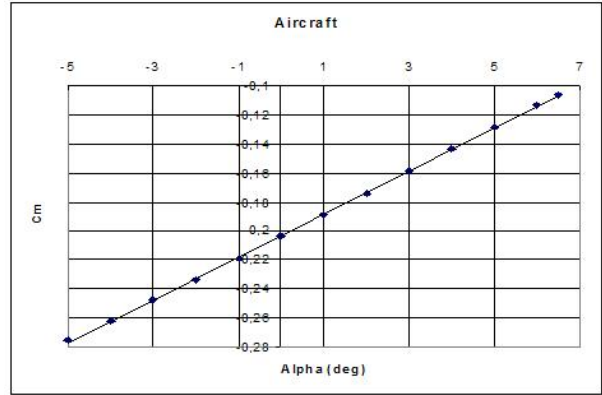
The test cases clearly explore the flight conditions in which the airplane has a linear aerodynamic behavior, *i.e.*, the aerodynamic coefficients change linearly with the AoA and canard deflection variations. The resultant aerodynamic coefficients and derivatives for the aircraft and canard are listed in Table 4. For higher or lower angles, unsteady solutions were found, but not completely simulated due to computational restrictions. An aspect that should be pointed out is the wing incidence angle of approximately 5 deg. used in the 14-Bis aircraft.

The plots in Figs. 3 and 4 carry much information about the aerodynamic performance. For example,  $C_{m\delta_p}$  corresponds to 153% of  $C_{m\alpha}$  and  $C_{L\delta_p}$  is just 9.3% of  $C_{L\alpha}$ , meaning that the canard seems to be effective to perform its principal function, the aircraft pitch control. However, a remarkable point is that the aircraft resultant moment increases with the AoA, meaning that the airplane is unstable what would, at least, demand great pilot effort to control the flight.

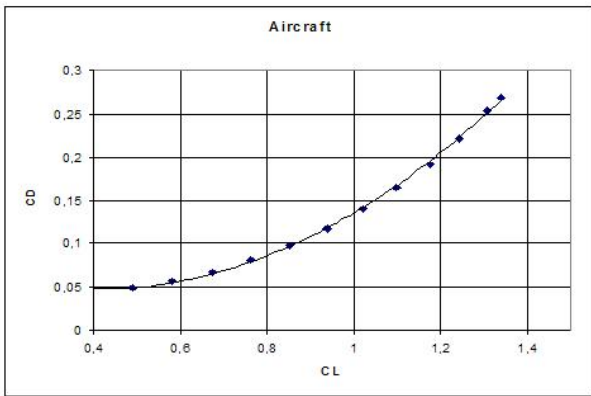
A detailed discussion about stability is addressed ahead. The downwash effect of the canard over the wing was also checked out, and, as expected, negligible variations in the wing aerodynamic coefficients were observed with different canard deflections. The inverse, *i.e.*, the upwash caused by the wing over the canard can be verified if one notes that the canard generates about 9.7 N of lift, without deflection, even though the canard



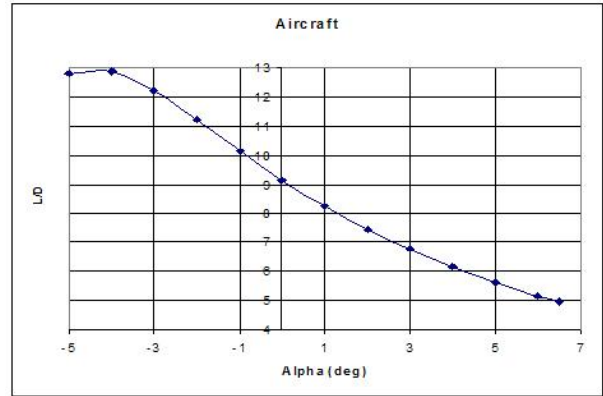
(a)  $C_L \times \alpha$  curve for the airplane.



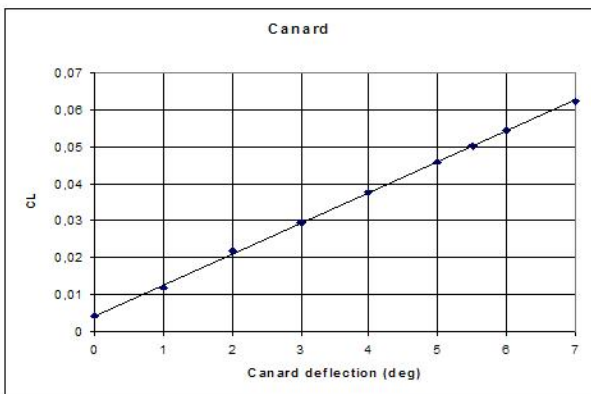
(b)  $C_m \times \alpha$  curve for the airplane.



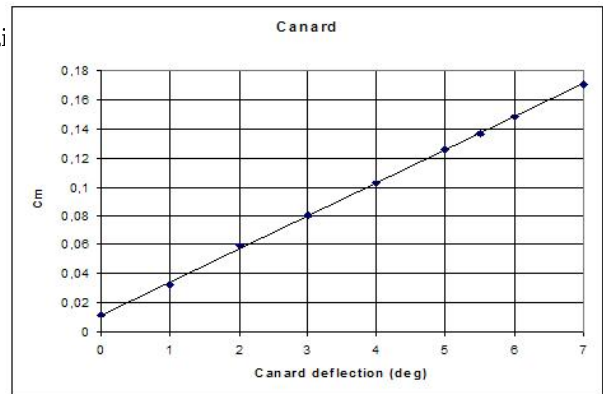
(c) Drag polar for the entire airplane.



(d)  $L/D \times \alpha$  curve for the airplane.



(a)  $C_L \times \delta_p$  curve for the canard.



(b)  $C_m \times \delta_p$  curve for the canard.

Figure 4: Aerodynamic coefficients for the canard keeping zero angle of attack for the airplane.

Table 4: Aerodynamic coefficients and derivatives of the airplane and control surfaces.

| AIRPLANE      |       | CANARD          |      |
|---------------|-------|-----------------|------|
| $C_{L\alpha}$ | 4.85  | $C_{L\delta_p}$ | 0.45 |
| $C_{m\alpha}$ | 0.85  | $C_{m\delta_p}$ | 1.31 |
| $C_{m_o}$     | -0.21 |                 |      |
| $C_{L_o}$     | 0.85  |                 |      |
| $C_{Y\beta}$  | -1.76 |                 |      |
| $C_{n\beta}$  | -1.20 |                 |      |
| $C_{l\beta}$  | -1.12 |                 |      |

is modeled by means of flat plates. This effect is not noticeable in terms of total lift, but a significant pitch moment about the aircraft CG is added, since the CG position was estimated to be placed between 7.0 m and 7.5 m from the aircraft nose.

The aerodynamic efficiency,  $L/D$ , for different angles of attack can be seen in Fig. 3(c). The loss of efficiency as the angle of attack increases is quite notable. For instance, a variation of 61% in the  $L/D$  value is found given the range of 12 deg. studied. This is most probably related to a large amount of induced drag produced by the aircraft.

In the fourth test case, the influence of lateral flow by varying sideslip angles on the airplane was evaluated. In doing so, some clues to analyze potential risks of a lateral flow, or even gusts could be tested. Just looking at the plots in the Fig. 5, the linear approximation for the stability derivatives seems perfectly reasonable and their values are listed in Table 3. As can be observed, the sideslip angle induces significant and equally important roll and yaw moments. Such a statement can be made because both coefficients have the same order of magnitude. This points out a coupling between roll and yaw moments, which is an underlying characteristic of this airplane. The numerical results have also shown that lateral flow exerts negligible influence on the longitudinal coefficients, namely  $C_L$ ,  $C_D$  and  $C_m$ , having a maximum relative variation of 3% along the sideslip angle range tested.

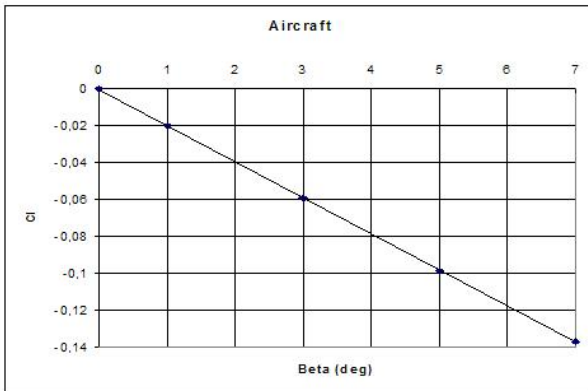
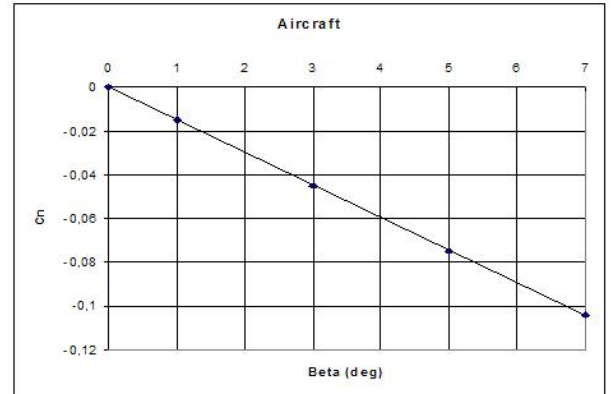

 (a)  $C_l \times \beta$  curve for the airplane.

 (b)  $C_n \times \beta$  curve for the airplane.

Figure 5: Aerodynamic coefficients for the airplane under sideslip.

In order to analyze the flight conditions, a linear aerodynamic model was used. The aerodynamic derivatives and coefficients shown in Table 4 are used to predict the lift, drag and moment coefficients as follow

$$C_L = C_{L_o} + C_{L\alpha}\alpha + C_{L\delta_p}\delta_p \quad (6)$$

$$C_M = C_{m_o} + C_{m\alpha}\alpha + C_{m\delta_p}\delta_p \quad (7)$$

$$C_D = 0.892 - 0.206C_L + 0.252C_L^2 \quad (8)$$

Before applying this methodology, its accuracy was verified. The model predictions were directly compared with the CFD data. The relative differences between the model and the CFD results were always less than 10%,

with the exception of the three highest canard deflection angles. Consequently, the linear model was adopted for the study of flight conditions because the accuracy fits under the expectations.

The exact CG position is unknown and, therefore, conclusions concerning the 14-Bis aircraft stability are only as good as the estimates of CG position. The stability criterium states that an airplane is stable if, when perturbed from its equilibrium condition, restorative moments bring the airplane back to the equilibrium condition. Estimations of the mass of each airplane component (Greco and Ribeiro, 2003) found a range between 7.0 m and 7.5 m for the CG position, measured from the airplane nose.

If the pitch moment derivative ( $C_{m\alpha}$ ), which comes from the curve  $C_m \times \alpha$ , is positive, the airplane is considered unstable, otherwise, stable for negative values and neutral for a zero value. The numerical results indicates an unstable condition for CG positions higher than 6.87 m. Therefore, the 14-Bis could be an unstable airplane if the estimated range for CG positions were right.

First, the authors would emphasize that unstable airplanes can fly, however their controllability is more difficult. Second, Santos Dumont could have changed the CG position by adding sufficient weights to turn the airplane stable.

The estimated flight conditions were studied considering the flight as being steady and level, *i.e.*, the speed derivative ( $\dot{V}$ ), the AoA derivative ( $\dot{\alpha}$ ), and the resultant moment at the center of gravity are all zero. Those constraints turn the differential system of equations for the longitudinal dynamics into a simplified nonlinear system with three equations and four unknown variables,

$$F_e \cos(\alpha_e) - D_e = 0 \quad , \quad (9)$$

$$L_e - mg + F_e \sin(\alpha_0) = 0 \quad , \quad (10)$$

$$C_{m0} + C_{m\alpha}\alpha + C_{m\delta_p} = 0 \quad , \quad (11)$$

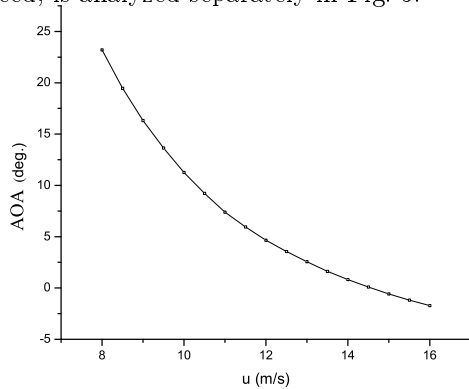
in which,

$$L_e = q_\infty S_w C_L \quad , \quad (12)$$

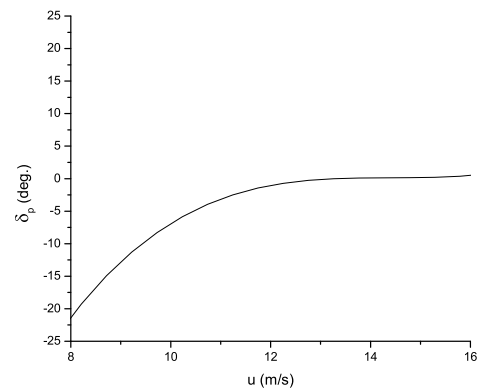
$$D_e = q_\infty S_w C_D \quad . \quad (13)$$

Here,  $q_\infty$  is the freestream dynamic pressure, given in its standard definition as  $q_\infty = \rho V^2/2$ ,  $S_w$  is the wing planform area, and  $mg$  is the airplane weight.  $C_L$  is the lift coefficient, and  $C_D$  is the drag coefficient, as shown in Eqs. 6 and 8, respectively. The remaining coefficients are all listed in Table 4. Moreover, the four unknown variables are flight speed ( $V$ ), AoA ( $\alpha$ ), canard deflection ( $\delta_p$ ) and required thrust ( $F_e$ ).

That system of equations does not have only one solution, but it has infinite solutions. The adopted procedure to study the steady flight condition is to find the equilibrium state for each flight speed. Figure 5 shows the necessary AoA and canard deflection for each flight speed. The third condition, the required propulsion for each speed, is analyzed separately in Fig. 5.

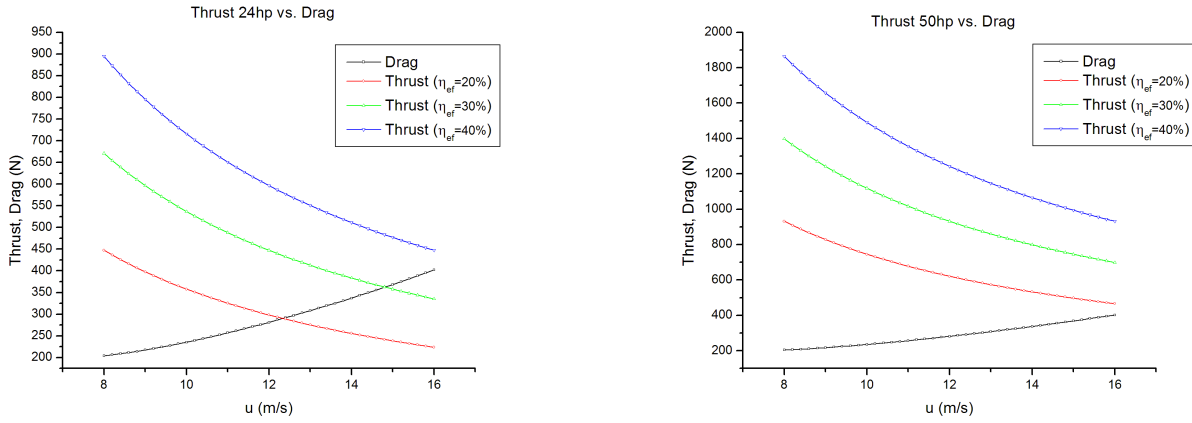


(a) AoA necessary to maintain permanent flight for each flight speed.



(b) Canard deflection required to maintain permanent flight for each flight speed.

Figure 6: Study of flight conditions parameterized by the flight speed.



(a) Drag and thrust dependence with velocity for the 24 hp engine.

(b) Drag and thrust dependence with velocity for the 50 hp engine.

Figure 7: Study of thrust requirements for sustained flight.

The adopted procedure to investigate the most probable flight condition consists in discarding high AoA and canard deflection, in which surely the airplane would experience stall, followed by an analysis of the propulsive requirements. In addition, the historical pictures and reports provide auxiliary clues that validate the numerical model.

The numerical results show that a sustained flight within the linear range is perfectly feasible. The suggested flight conditions are AoA between 5 deg. and 10 deg., canard deflection between -5 deg. and 5 deg., as well as, the flight speed between 11 m/s and 14 m/s. Looking at the historical picture in Fig. 1, the observable flight condition evidence AoA in the range 5 deg. to 10 deg. and an almost imperceptible canard deflection. Such condition could be attested in Fig. 6.

The next step verifies the propulsive requirements to overcome the generated drag. It is important to note that the thrust produced by the engine decreases as the flight speed increases. As the true propulsive efficiency ( $\eta_p$ ) is unknown, three isolines of different  $\eta_p$ , with values 20 %, 30 % and 40 %, are considered in the present analyses, considering both the 24 hp and the 50 hp engines. Furthermore, one should also note that both engine power and propulsive efficiency values are in agreement with the historical records (Vilares, 1956).

The propulsive analysis with the 24 hp engine in Fig. 5(a) permit to say that the flight is viable, however having very restrictive conditions. For example, for speeds larger than 12.4 m/s, flight is not possible if the actual propulsive efficiency of the aircraft was closer to the lower limit here considered, *i.e.*, 20 %. Some factors should be carefully observed about drag and thrust estimated values. First, due to geometric simplifications, the CFD drag results here reported are probably lower than the actual drag in flight. As a result, the drag curves in Figs. 5(a) and 5(b) should be shifted upwards, further restricting the admissible flight speed range and bringing the probable flight speed closer to the historically reported one. Moreover, during takeoff, ground effect causes additional drag and lift forces.

The fifth test case set in Table 4, detected an increase of 6 % to the lift and only 3 % to the drag relative to the condition without ground effect. The power deficiency of the 24 hp engine became evident on September 13, 1906, during a flight attempt, when the aircraft, in spite of some jumps, was unable to take off. During the following experiments, a new and more powerful engine was selected. Its nominal power was 50 hp at 1500 rpm (Vilares, 1956). The propulsive analysis with the new 50 hp engine clearly evidences that the propulsive restriction was overcome, allowing sustained flight in the complete speed range showed, even with the smaller value of propulsive efficiency.

## 6. Conclusions

The present work has used CFD techniques to perform an aerodynamic evaluation of the 14-Bis aircraft configuration. The historical flight conditions are simulated using a finite volume method and solving the RANS equations with the Menter SST turbulence model. A geometrically simplified model of the aircraft is used and the results obtained so far seem to corroborate many of the historical reports.

The results presented in the previous section confirmed why the 24 hp engine was unable to allow the 14-Bis

aircraft to take off during the first flight attempt on September 1906. Therefore, the engine change, selecting a more powerful one with 50 hp, is clearly justified. Based on the present calculations, it is difficult to believe that 10.21 m/s was the true airspeed of the aircraft, because the AoA vs. speed curve, that was generated during the simulations, indicates that an AoA of approximately 10 deg. is required to maintain sustained flight at this speed. If one adds such an aircraft angle of attack to the 5 deg. wing incidence, it is clear that the airplane would be in a stall condition. An acceptable flight speed, assuming a 5 deg. angle of attack, seems to be around 12 m/s. Such speed could be reached more easily when flying against the wind direction. In any event, it can be stated, based upon the present numerical results, that the flight speeds should have been higher than 12 m/s. The results further indicate that, considering the 50 hp engine, the availability of thrust was not a limitation to the flight.

The analysis of longitudinal static stability considered the linear regime and it has shown that the estimated position of the neutral point is coherent with historical reports. Moreover, the parametric tests demonstrate that small center of gravity position variations, around the historical point, could render the aircraft statically unstable. This study concerning longitudinal static stability has emphasized that the CG position seems to be a critical factor for the 14-Bis flight. However, it must be stated that, as cited in Greco and Ribeiro (2003), Santos Dumont used to modify the CG position by adding weights to alter the CG location, leading the aircraft to a stable condition.

A well defined range of flight conditions is found, namely AoA between 5 and 10 deg., canard deflections between  $-5$  and 5 deg. and flight speeds between 11 and 14 m/s. This indicates that the possible flight conditions are, in fact, wider than the historical values usually cited. Other important aircraft characteristics are identified, such as the roll and yaw coupling when subjected to lateral flow.

## 7. Acknowledgments

The authors are indebted to Prof. Paulo Greco, from Escola de Engenharia de São Carlos, Universidade de São Paulo, who provided the geometrical CAD model, and to Mr. Marcus Reis, from Engineering Simulation and Scientific Software, ESSS, who provided support and licences for all used software. The authors acknowledge the partial support of Conselho Nacional de Desenvolvimento Científico e Tecnológico, CNPq, through the Integrated Project Research Grants No. 501200/2003-7 and 502053/2004-6. The support of Fundação de Amparo à Pesquisa do Estado de São Paulo, FAPESP, through the Research Grant No. 2000/13768-4, is also gratefully acknowledged.

## 8. References

- Bitencourt, L.O., Freitas, R.M, Pogorzelski, G., and Azevedo, J.L.F., 2005, “Advanced CFD Analysis of 14-Bis Aircraft,” *Proceedings of the 18th ABCM International Congress of Mechanical Engineering – COBEM 2005*, Ouro Preto, MG.
- CFX, 2005, [www-waterloo.ansys.com/cfx/](http://www-waterloo.ansys.com/cfx/).
- Cummings, R.M, Giles, M.B., and Shrinivas, G.N., 1996, “Determination of Drag from Three-Dimensional Viscous and Inviscid Flowfield Computations,” AIAA Paper No. 96-2482, of the 14th AIAA Applied Aerodynamics Conference, New Orleans.
- Field, D.A., 1987, “Laplacian Smoothing and Delaunay Triangulations,” *Communications of Applied Numerical Methods*, Vol. 4, pp. 709-712.
- Greco, P.C., and Ribeiro, M.L., 2003, “A Study of the Aerodynamic, Stability and Control Characteristics of the 14-Bis Aircraft,” Technical Report FAPESP No. 01/11158-7, Escola de Engenharia de São Carlos, Universidade de São Paulo, São Carlos (in Portuguese, original title is “Estudo das Características Aerodinâmicas, de Estabilidade e de Controle do 14-Bis”).
- ICEM-CFD, 2005, <http://www.icemcf.com/icemcf.html>.
- Jones, W. P., and Launder, B. E., 1972, “The Prediction of Laminarization with a Two-Equation Model of Turbulence,” *International Journal of Heat and Mass Transfer*, Vol. 5, pp. 301-314.
- Menter, F.R., 1994, “Two-Equation Eddy-Viscosity Turbulence Models for Engineering Applications,” *AIAA Journal*, Vol. 32, No. 8, pp. 1598-1605.
- Vilares, H. D., 1956, *Quem Deu Asas ao Homem*, Instituto Nacional do Livro, Rio de Janeiro.

## 9. Author Rights

Authors are the sole responsible for the contents of their papers.